

# The effect of Ganges river basin irrigation on pre-monsoon rainfall

J. K. Fletcher<sup>1,2</sup>  | C. E. Birch<sup>1</sup>  | R. J. Keane<sup>1,3</sup>  | C. M. Taylor<sup>4</sup>  | S. S. Folwell<sup>4</sup> 

<sup>1</sup>School of Earth and Environment,  
University of Leeds, Leeds, UK

<sup>2</sup>National Centre for Atmospheric  
Science, University of Leeds, Leeds, UK

<sup>3</sup>Met Office, Exeter, UK

<sup>4</sup>UK Centre for Ecology and Hydrology,  
Wallingford, UK

## Correspondence

J.K. Fletcher, 71–75 Clarendon Road,  
University of Leeds, Leeds LS2 9PH, UK.  
Email: j.k.fletcher@leeds.ac.uk

## Funding information

Newton Fund WCSSP India WP2 Lots 3  
and 4 (IMPROVE), and the UK NERC  
INCOMPASS grant at University of Leeds  
(NE/L013843/1) and Centre for Ecology  
and Hydrology, Grant/Award Numbers:  
(NE/L013819/1)

## Abstract

The first experiment studying the effect of irrigation on pre-monsoon rainfall in India using a high-resolution convection-permitting model has been carried out. This study includes both short (3-day) experiments and month-long free-running simulations, enabling investigation of the effect of irrigation on mesoscale circulations and associated rainfall. In the pre-monsoon, it is found that irrigation increases rainfall in our simulations. Intriguingly, the rainfall increase found in the high-resolution model mostly occurs on the mountains near the irrigation rather than over the irrigated region itself. This is because our applied irrigation is in low-lying regions, and so it enhances the mountain-valley flows leading to enhancement of diurnally driven orographic rainfall. Because Ganges basin irrigation occurs near mountains which already have some of the highest rainfall rates in the world, and which are subject to flash flooding and landslides, this has significant implications for hazards in mountainous regions during the pre-monsoon and early monsoon period.

## KEYWORDS

convection, India, irrigation, monsoon, precipitation

## 1 | INTRODUCTION

Northern India, particularly the Ganges basin, has some of the strongest precipitation–soil moisture coupling in the world (Koster *et al.*, 2004). Understanding how atmospheric circulation and rainfall patterns respond to and feed back on irrigation patterns is therefore essential to improving our physical understanding and prediction of the South Asian monsoon. The Ganges River catchment plain supports roughly 400 million people on one million square km of land (Islam, 2007). This river catchment is highly managed, with more than half of the land equipped

for irrigation, generating a profound perturbation on the surface conditions. Douglas *et al.* (2006) estimated that irrigation produces a 17% increase of surface latent heat fluxes over India compared to pre-agricultural times, and Lee *et al.* (2009) found statistically significant increases in surface latent heat fluxes in the late 20th century which were associated with increases in the spatial extent of irrigation. Niyogi *et al.* (2010) used causal data analysis methods on satellite retrievals of normalised differential vegetation index and suggested that pre-monsoon increases in vegetation led to decreases in monsoon rainfall. However, irrigation is not generally considered in weather and climate

models, and Saeed *et al.* (2009) attributed a long-standing warm bias over the South Asian heat low region in many general circulation models (GCMs) to the lack of representation of irrigation in the Indus river basin.

Observational studies (Douglas *et al.*, 2006, Lee *et al.*, 2009) suggest the importance of irrigation for the surface energy balance and for rainfall, but the effect of irrigation must be disentangled from other anthropogenic forcings and internal variability. This separation is somewhat simpler in a modelling framework (Shukla *et al.*, 2013). Previous modelling studies of the effects of irrigation in India have used coarse-resolution (grid spacing on the order of 100 km) GCMs, or occasionally regional climate models (grid spacing on the order of tens of km), in which cumulus convection is parametrized. These studies have found that large-scale land surface cooling due to widespread irrigation weakened the monsoon circulation and reduced rainfall over central India (Saeed *et al.*, 2009; Puma and Cook, 2010; Cook *et al.*, 2014; Chou *et al.*, 2018) and delayed the monsoon onset by about a week (Guimberteau *et al.*, 2011). These studies have attributed the surface cooling to evaporation (Puma and Cook, 2010), increases in cloud cover (Sacks *et al.*, 2008), or both (Cook *et al.*, 2014; Chou *et al.*, 2018). Shukla *et al.* (2013) argued that irrigation, combined with global surface temperature increases, is acting to reduce interannual variability in the Indian summer monsoon.

While it is reasonable to expect that the continental-scale circulation response to land surface temperature changes would be well-represented in a GCM, at least qualitatively if not quantitatively, there is less confidence that GCMs, or regional models with parametrized convection, will produce the correct rainfall response, both to the large-scale circulation changes and to the local-scale changes in surface properties, particularly when convection is parametrized. This was first identified by Hohenegger *et al.* (2009), who found that a coarse-resolution model with parametrized convection favoured rain over wet soils while the high-resolution convection-permitting version of the same model favoured rainfall over dry soils. They attributed this to parametrized convection's insensitivity to stable layers at the boundary-layer top and poor representation of the difference in thermal buoyancy above wet and dry soils. Taylor *et al.* (2013) found that a weather forecasting model (run at higher resolution than the GCM studies discussed above) with parametrized convection failed to reproduce the observed relationship between soil moisture heterogeneity and convection in the Sahel. The model favoured convection over wet soils when observations of this environment – as well as those of north-western India – show that convection over wet soil is suppressed (Taylor *et al.*, 2012; Barton *et al.*, 2020). However, when Taylor *et al.* (2013) turned off deep convective

parametrization, the same model reproduced the correct soil moisture–precipitation feedback, even at the relatively coarse horizontal resolution of 12 km. These results suggest that high-resolution convection-permitting models can uncover important aspects of the relationship between irrigation and monsoon rainfall, particularly the aspects that are driven by local convective and mesoscale processes and how those processes respond to surface forcing. While some regional modelling studies have been done (e.g., Douglas *et al.*, 2009; Saeed *et al.*, 2009; Tuinenburg *et al.*, 2014), these are still relatively coarse resolution and have parametrized convection.

In this paper, we make use of recent advances in high-resolution convection-permitting atmospheric modelling to study the effect of irrigation on mesoscale circulations and associated rainfall patterns over northern India. To our knowledge, this paper is the first to use convection-permitting models to examine the effects of irrigation over India, allowing us to resolve some of the topographic circulations in the region as well as to test the effect of irrigation in a framework which we know has a reliable relationship between soil moisture and precipitation.

Our study was carried out for the pre-monsoon period in the Gangetic Plain region, so we show the mean circulation in that period in Figure 1. We chose the pre- and

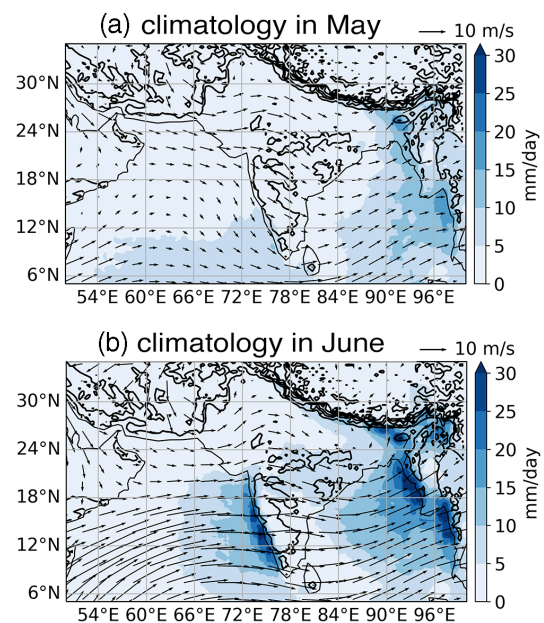


**FIGURE 1** Mean 10 m surface winds from ERA5 (Hersbach *et al.*, 2020) for 2001–2020 and rainfall from GPM IMERG (Huffman *et al.*, 2015) for 2000–2020 in (a) May and (b) June for the South Asian region. Elevation is also shown with contour intervals of 500 m. The domain shown here is the same as that of the regional model used in this study [Colour figure can be viewed at [wileyonlinelibrary.com](http://wileyonlinelibrary.com)]

**TABLE 1** Summary of MetUM simulations used

Name	Description	Duration	Soil moisture
Long run control	Standard MetUM tropical convection-permitting	4 June–1 July 2012	Initialised from climatological JULES outputs
Long run irrigated	Standard MetUM tropical convection-permitting	4 June–1 July 2012	As long run control, plus strongly perturbed based on observed LST; reinitialised each night
Short runs control	10 simulations, standard MetUM tropical convection-permitting	3-day periods in May, June 2016	Initialised from JULES forced with 2016 observations
Short runs irrigated	10 simulations, standard MetUM tropical convection-permitting	3-day periods in May, June 2016	As short runs control, plus refined LST-based perturbations

early monsoon period for this study because we expect that to be the time during which the effects of irrigation are strongest, because isolated convective showers dominate and convection is less organised by the large-scale circulation than after monsoon onset, and because unirrigated soil is drier than during the monsoon, increasing the contrast between irrigated and unirrigated soil. While at this time there are large differences in both circulation and rainfall over the west coast of peninsular India, the Bengal region and Myanmar, the monsoon onset in northern India typically does not arrive until late June and so the circulation and rainfall in May and June are fairly similar to each other (Figure 1). Over the Gangetic Plain, low-level northwesterlies prevail except along the foothills of the Himalayas, where the winds blow southeasterly as the monsoon trough develops. Most pre-monsoon rainfall over the north Indian monsoon core zone (Rajeevan *et al.*, 2010) falls as isolated convective showers rather than as part of synoptic systems such as monsoon lows, which provide the bulk of rainfall to this region during the monsoon season proper (Hunt and Fletcher, 2019).

Section 2 describes the simulations and our approach to specifying the land boundary conditions associated with irrigation. The details of the latter are presented in the Appendix. We show the effect of irrigation on the mean rainfall and then explore its effect on the diurnal cycle of rainfall, especially the diurnal cycle of orographic precipitation, in Section 3. We reconcile our results with previous work in Section 4 and discuss future work which might further clarify issues raised here.

## 2 | DATA AND METHODS

### 2.1 | Simulations

We carried out simulations with the UK Met Office Unified Model (MetUM), with a horizontal resolution of 4.4 km and with the deep convection parametrization switched off. These simulations were over a regional

domain covering South Asia from 5° to 35°N and from 50° to 100°E, as illustrated in Figure 1. The regional model was driven on the boundaries by analyses and short-range simulations from the global MetUM (GA6.1/GL6.1). Six-hour global simulations were executed every 6 hr, starting from the Met Office operational analyses, to provide boundary conditions that were updated every hour. The regional simulations were initialised using the global analysis (downscaled to 4.4 km) only once at the start so that, other than the forcing at the boundaries, the circulation within the regional domain was able to develop internally for the duration of each simulation. The regional model is described by Bush *et al.* (2020); our set-up was identical to that applied over India by Martin *et al.* (2020), except for the use of specially produced ancillary files used for soil moisture initialisation, as described in Section 2.2.

We carried out two basic types of simulation which differ by duration and by the magnitude of the irrigation forcing applied, summarized in Table 1. The first type was a continuously-run experiment over the month of June 2012, prior to the local onset for most of northern India. For this simulation type, we carried out a control experiment and an irrigation experiment, described in Section 2.2. The month-long experiment was a preliminary study. In this simulation we found that the intensity of the soil moisture forcing was unrealistically strong in comparison to remotely sensed data (Appendix), and we recognized that some of the differences between the control and irrigation experiments in a month-long run is due to internal variability.

For the above reasons, we also generated and analysed a suite of ten non-overlapping three-day simulations, in which the synoptic-scale circulation was constrained; in other words, the much shorter length of the simulations reduced differences due to synoptic evolution. These simulations were carried out over non-overlapping three-day periods in May and June 2016, prior to the onset of the monsoon in northern India. We focused on synoptically undisturbed times because synoptic-scale organisation of rainfall, as happens in e.g., a monsoon low pressure

system, will at least partly mask the local effects of irrigation. As with the month-long simulation, we carried out control and irrigated experiments for each period simulated, and this method is described in Section 2.2. In all figures below, the first day of each three-day simulation was excluded, unless stated otherwise, to allow for both atmospheric and soil moisture spin-up.

Our analysis focuses largely on the short simulations due to their more realistic soil moisture forcing and better-constrained synoptic variability. We also include some results from the month-long simulation, focusing on the qualitative response particularly where it is consistent with the short runs, because a consistent response between these two types of simulations is a more robust result. The month-long experiment is useful for providing an estimate (likely a lower bound) on the time-scale of the circulation response to irrigation.

## 2.2 | Soil moisture perturbations

The focus of this study is on the atmospheric impact of irrigation rather than irrigation processes per se. At this time of the year, irrigation takes the form of flooding of fields from the network of channels across the region. Such processes are not currently represented in the MetUM. To represent the impact of irrigation on surface fluxes, we therefore chose to introduce additional soil moisture into the land surface model. The amount of soil moisture was varied across the domain, consistent with the heterogeneous nature of irrigation in northern India. We based this distribution on satellite climatological land surface temperatures (LSTs; full details are provided in the Appendix). During the pre-monsoon season, evapotranspiration is strongly constrained by soil moisture. The surface energy balance is therefore highly sensitive to the presence of additional water applied by farmers, which maintains evaporation at its potential rate (Bhat *et al.*, 2020). As a result, prior to the monsoon, areas with irrigation can exhibit a suppression of daytime LST by as much as 10 K compared to nearby unirrigated fields (Figure A1).

We developed a simple linear method to translate climatological LST into soil moisture increments (Figure A2). This was based on two subjectively identified thresholds. For locations with LSTs at or below the lower threshold of 313 K, the surface was considered to be fully irrigated, whilst areas warmer than 319 K had no irrigation water applied. The resulting irrigated soil moisture increments were superimposed on a control soil moisture field computed from running the MetUM's land surface scheme forced by observations.

In our first attempt to represent irrigation, used in the month-long simulation, we used climatological forcing for

the offline land model, and fully irrigated grid boxes had their soil moisture set close to saturation. The combination of the offline model output and irrigation increments were used to reinitialise the MetUM's soil moisture across the entire domain each night. We found that, with this approach, the atmospheric model simulated excessively low LSTs in irrigated regions when compared to the observational climatology (Figure A3). For our second attempt, used in the short runs, we reduced the soil moisture in fully irrigated grid cells to a level that limited evaporation direct from the bare soil, whilst still permitting transpiration to occur without constraints from soil moisture. The control soil moisture field was created using observational forcing for the period in question (rather than climatology). Unlike in the month-long irrigated simulation, once initialised, the soil moisture in the three-day runs was allowed to evolve freely in response to the model physics.

This approach to identifying where irrigation has taken place offers simple objective identification of areas which are irrigated during the pre-monsoon season, including some measure of the degree of irrigation occurring. Our LST-based method suggests far more irrigation occurring in the lower Gangetic plain than was used during the pre-monsoon period by Chou *et al.* (2018). However, this method does not work well for high elevations, and so we limit our study to the low-lying Gangetic plain and do not represent Indus river region irrigation.

## 2.3 | Other methods

Prior to plotting in maps, the data were smoothed using the Python 2.7 SciPy package's Gaussian filter module, with sigma values ranging from 1 to 6 ([https://docs.scipy.org/doc/scipy-0.14.0/reference/generated/scipy.ndimage.filters.gaussian\\_filter.html](https://docs.scipy.org/doc/scipy-0.14.0/reference/generated/scipy.ndimage.filters.gaussian_filter.html); accessed 29 November 2021). Smoothing did not affect the magnitude of the plotted variables, but it filtered out some of the noise to aid interpretation. The statistical significance of differences in rainfall between the control and irrigation simulations were tested with the Wilcoxon–Mann–Whitney test (Mann and Whitney, 1947), employing a non-parametric test due to the non-Gaussian distribution of rainfall.

# 3 | RESULTS

## 3.1 | The effect of irrigation on daily mean rainfall and circulation

The effect of irrigation on mean rainfall and large-scale circulation in the experiments is shown in Figure 2. In both the month-long simulation and the mean of the short

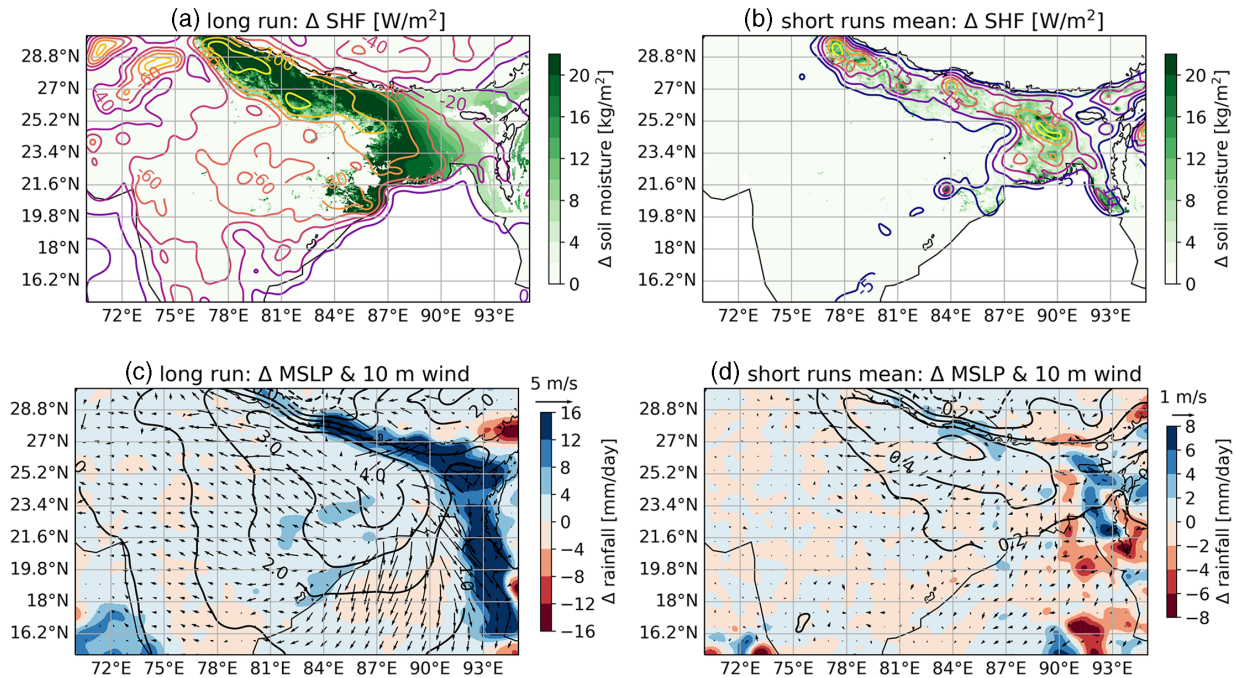


**FIGURE 2** The mean difference between irrigation and control simulations for (a, b) the surface soil moisture perturbation (shading) and surface sensible heat flux ( $\Delta$  SHF, positive up, contours), and (c, d) rainfall (shading), mean sea level pressure (MSLP, contours), and 10 m winds (arrows). (a, c) show the month-long experiments and (b, d) show the mean of the ten short experiments. The contour interval in (a) is  $-20 \text{ W}\cdot\text{m}^{-2}$  and in (b) is  $-5 \text{ W}\cdot\text{m}^{-2}$  (with first contour  $-5 \text{ W}\cdot\text{m}^{-2}$ ). The 1,000 m elevation is indicated by a thin black contour [Colour figure can be viewed at [wileyonlinelibrary.com](http://wileyonlinelibrary.com)]

simulations, irrigation substantially reduces surface sensible heat fluxes (with a near-equal-magnitude increase in surface latent heat fluxes, not shown), weakens the monsoon trough in northeast India and Bangladesh, and mostly increases rainfall. The magnitude of the decrease in surface sensible heat fluxes over the irrigated region exceeds  $80 \text{ W}\cdot\text{m}^{-2}$  in the long experiment and  $10 \text{ W}\cdot\text{m}^{-2}$  in the short experiments. The mean sea level pressure (MSLP) increases by up to 4 hPa in the long run and nearly 1 hPa in the short run, weakening the pressure gradient in the monsoon trough region. For reference, this pressure gradient is observed to be roughly 2–3 hPa over the irrigated Gangetic Plain region (e.g., figure 1 of Turner *et al.*, 2020) during the monsoon, and would be weaker during the pre-monsoon. The effect is therefore substantial in both types of simulation but is much stronger, as expected, in the month-long experiments.

In the month-long experiments, the difference in MSLP between the control and irrigation experiments steadily increased after the first few days, then continued to increase slightly over the course of the month, as shown in Figure 3. The development of the monsoon trough is key to the onset of the monsoon because the pressure gradient within the trough drives the large-scale low-level circulation which brings moisture from the Bay of Bengal to central India. This suggests that, had these simulations been carried out over a full monsoon season, irrigation

could have substantially delayed the monsoon onset in northern India, as seen in the previously mentioned GCM studies, even as irrigation increased pre-monsoon rainfall.

We calculated convective available potential energy (CAPE), convective inhibition (CIN), and the height of the lifting condensation level (LCL) within selected regions. These calculations are not shown but we summarise their results here. We found that irrigation in the short simulations produced low-level (i.e., about 900 hPa) increases of specific humidity between 0.5 and  $1.0 \text{ g}\cdot\text{kg}^{-1}$  in irrigated regions throughout the domain, with corresponding reductions in CIN and increases in CAPE. However, the only irrigated places where rainfall substantially increased were near the northern east coast of India. This is because at this time of year, the boundary layer in most of the irrigated region is still very dry, with an LCL of about 650 hPa in our simulations. The perturbation added by irrigation was not enough to lower the LCL to heights necessary to expect rainfall. Thus, in the irrigated region, the effect of irrigation was limited by mean state humidity.

The rainfall response to the irrigation changes is much greater in the long run than in the short run, but it is unclear whether this is due to the length of the simulation or the magnitude of the forcing. To explore this further, we examine time series of rainfall and a few surface variables over the monsoon trough region, defined here as

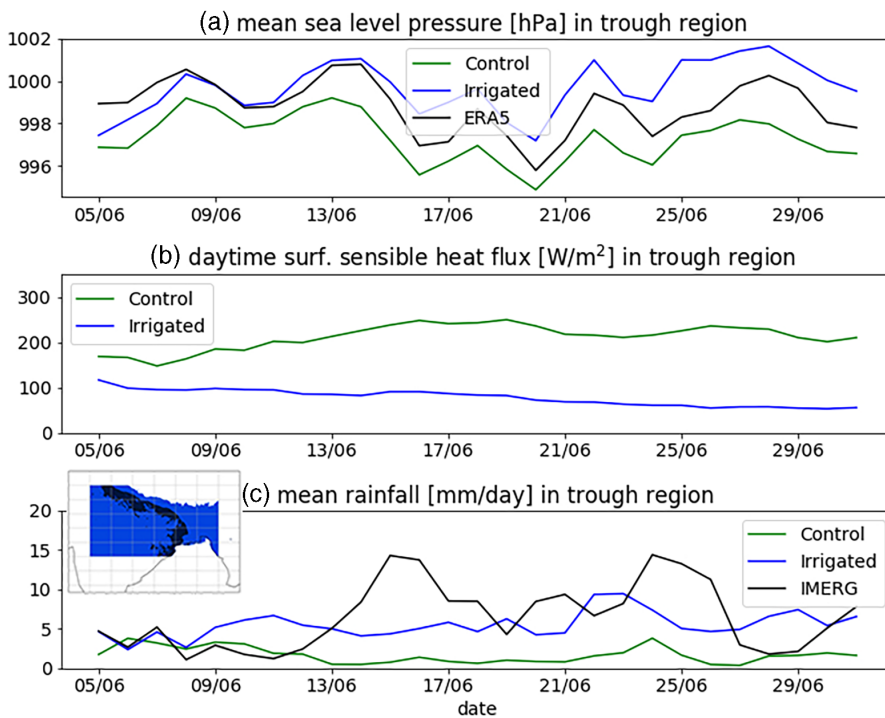


**FIGURE 3** Time series of daily mean values of (a) MSLP, (b) daytime surface sensible heat flux, and (c) rainfall for the monsoon trough region in the long simulations. (b) shows sensible heat fluxes averaged from 0600–1800 local time only. The inset map shows the region over which the averaging was done in medium shading, with the irrigated region in dark shading [Colour figure can be viewed at [wileyonlinelibrary.com](http://wileyonlinelibrary.com)]

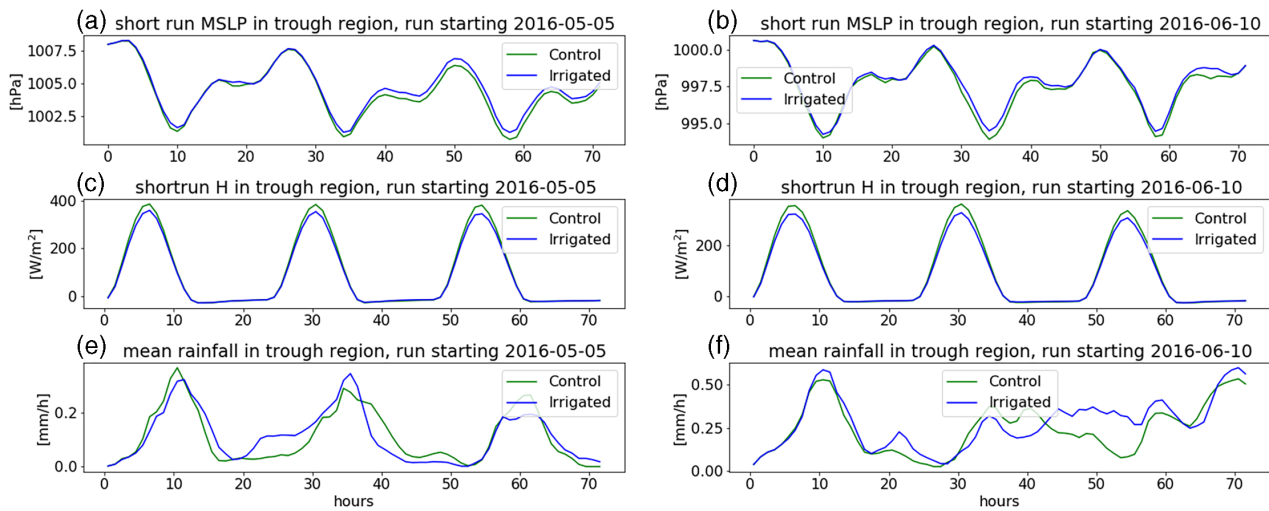


**FIGURE 4** Time series of half-hourly values for the monsoon trough region in two selected examples of the short simulations. The region over which the averaging is calculated is as in Figure 3. In (c, d) H is surface sensible heat flux [Colour figure can be viewed at [wileyonlinelibrary.com](http://wileyonlinelibrary.com)]

the area  $75^{\circ}$ – $93^{\circ}$ E,  $20^{\circ}$ – $30^{\circ}$ N, at elevations below 2,000 m, in Figures 3 and 4.

Figure 3 shows the time-scale over which the long simulation control and irrigation experiments become substantially different from each other. For reference, the MSLP in ERA5 (Hersbach *et al.*, 2020) and the rainfall from GPM IMERG<sup>1</sup> (Huffman *et al.*, 2015) are also shown.

<sup>1</sup>Global Precipitation Measurement; Integrated Multi-satellite Retrievals for GPM

The first day has been excluded due to rapid adjustments in MSLP and rainfall that occur on that day. Given the model's freedom to evolve synoptically, we do not expect day-to-day rainfall agreement and show IMERG only to give a sense of the overall rainfall bias in the model. The irrigation experiment has both MSLP closer to ERA5 (for the first 10 days of simulation) and rainfall closer to IMERG than control, consistent with Barton *et al.* (2020), who showed that lack of representation of irrigation affected MSLP bias over the three-day evolution of a

forecast. However over the course of the simulation a positive MSLP bias develops due to the too-cool surface, and the dry bias relative to IMERG observations persists.

From day 2 there is already a mean difference in MSLP of about 1 hPa between control and irrigation over the entire monsoon trough region, with a corresponding reduction of surface sensible heat fluxes in excess of  $50 \text{ W}\cdot\text{m}^{-2}$  in the irrigation experiment. However, the rainfall difference between the two experiments is small until about day 6 of the simulation (9 June), when the irrigation simulation begins to rain systematically more than the control experiment, with corresponding increases in the difference in MSLP and surface sensible heat fluxes. Inspection of the spatial distribution of the rainfall showed that this systematic increase occurred to the south of the irrigated region (not shown). This is a region where the prevailing pre-monsoon winds are from the extremely arid northwest (Figure 1b), but this flow is weakened in the irrigated simulation (Figure 2c), permitting the incursion of moisture from the Bay of Bengal. There is a positive feedback in which the slight weakening of the nascent monsoon trough in the first days of the simulation permitted more widespread rainfall beyond the irrigated region, resulting in widespread wetting of non-irrigated soil. Subsequent reductions in surface sensible heating further weakened the development of the monsoon trough. Unlike the short experiments, in the month-long experiments the surface sensible heat fluxes are reduced far outside of the irrigated region, as can be seen by comparing Figures 2a, b.

The effects seen in the month-long runs also appear in the mean of the short simulations, but they are less pronounced due to both the shorter integration times – as discussed above, the circulation response time-scale is on the order of 5 days – and, probably more importantly, the weaker forcing (compare the shading in Figure 2a, b). Figure 4 demonstrates how much more modest the forcing and response are in the short simulations than in the long ones. However, this is averaged over the entire monsoon trough region; Figure 2b shows that the most irrigated regions in the short runs have average reductions of surface sensible heat flux in excess of  $20 \text{ W}\cdot\text{m}^{-2}$ .

### 3.2 | The effect of irrigation on orographic precipitation and the diurnal cycle

For the remainder of this paper we focus on the mesoscale physical processes that respond to irrigation and how that affects rainfall. For this we limit our work to the more realistic and more constrained set of short runs.

Irrigation changes not just the large-scale land–sea contrast but also mesoscale contrasts between irrigated and unirrigated regions. We expect that this change in mesoscale temperature gradients will affect the diurnal cycle of circulation and rainfall. Mountainous regions are particularly likely to have diurnal cycles of rainfall associated with diurnally varying mountain-valley flows. Close inspection of the relationship of rainfall anomalies to the 1000 m contour in Figure 2 suggests that most rainfall increases in the irrigation simulations occur near mountains, especially along the Himalayan foothills and the Meghalaya plateau region, rather than on the irrigated regions themselves. We confirm that irrigation has an important effect on rainfall on nearby mountains by computing the mean diurnal cycle over three land surface sub-regions within the Gangetic plain region for the short runs. These sub-regions are: the irrigated region, where the soil moisture perturbation exceeded  $5 \text{ kg}\cdot\text{m}^{-2}$ ; the adjacent region, which is close to the irrigated region and is below 300 m elevation; and the orographic region, which is near the irrigated region and is at elevation exceeding 300 m. Figure 5 shows that the most substantial and statistically significant changes are as follows: increases on

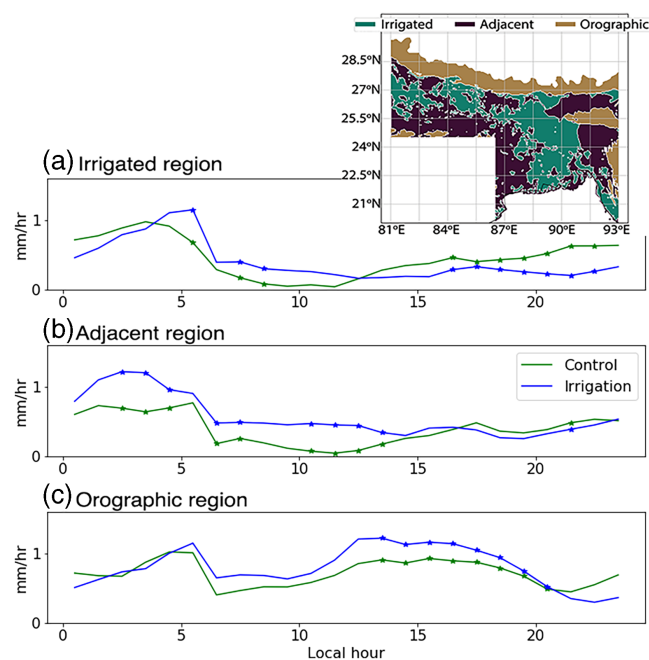


**FIGURE 5** The diurnal cycle of rainfall in (a) the irrigated region, identified by a change in soil moisture perturbation greater than  $5 \text{ kg}\cdot\text{m}^{-2}$ , (b) regions near the irrigated region at elevation below 300 m, and (c) orographic regions identified as elevation greater than 300 m. Stars indicate that the difference between control and irrigation rainfall is statistically significant at 95% confidence using a non-parametric rank-sum test [Colour figure can be viewed at [wileyonlinelibrary.com](http://wileyonlinelibrary.com)]

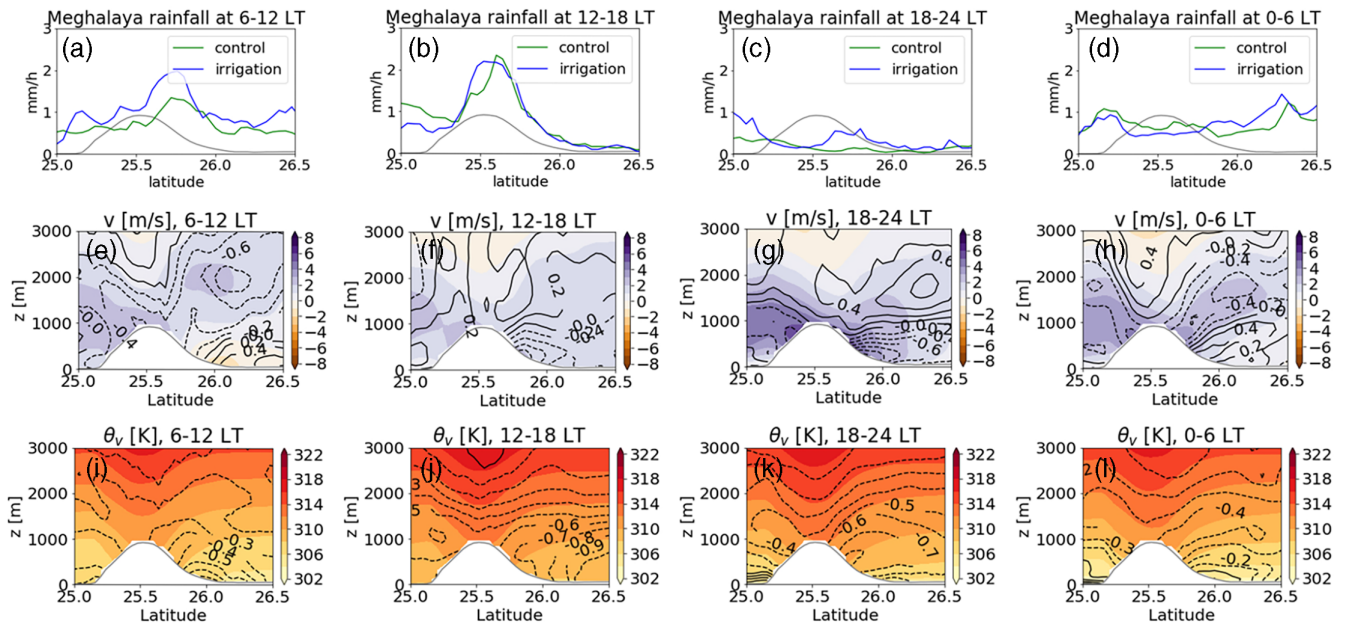


**FIGURE 6** The diurnal cycle of (a–d) rainfall, (e–h) meridional winds, and (i–l) buoyancy expressed as  $\theta_v$ , in the Meghalaya region, where irrigation produced the largest rainfall increase. In (a–d), the grey line indicates the mountain height (in km) to aid interpretation. In (e–l), shading indicates the mean from the control simulations while contours indicate the irrigation minus control change [Colour figure can be viewed at [wileyonlinelibrary.com](http://wileyonlinelibrary.com)]

the orographic region of roughly 10–30% in the daytime; decreases in the afternoon and at night over the irrigated region which are partially compensated by increases in the morning; and increases of roughly 30% in the morning on the adjacent region, largely at the base of the mountains.

Because these mountainous regions are vulnerable to extreme rainfall impacts such as flash floods and landslides, we further investigate the physical mechanisms behind the changes in this section, with particular attention to the Meghalaya Plateau.

### 3.2.1 | The Meghalaya Plateau

The effect of irrigation on the diurnal cycle in the Meghalaya Plateau region in the short simulations is explored in more detail in Figure 6. The Meghalaya plateau is south of the Himalayas and north of Bangladesh, at about 89.5–92.5°E, 25–26°N. In the morning, rainfall is particularly enhanced on the northern flank of the plateau (Figure 6a). In the afternoon (Figure 6b), the rainfall increase shifts to the peaks of the plateau, and at night the anomalous rainfall shifts to the lower flanks of the plateau and the lowlands to its north and south (Figure 6c,d).

This diurnal oscillation in the location of the rainfall anomaly can be partly understood by examining

Figure 6i–l, which show contours of virtual potential temperature

$$\theta_v = T \left( \frac{p_0}{p} \right)^{\frac{R_d}{C_p}} (1 + 0.61r_v),$$

where  $T$  is temperature;  $p_0$  and  $p$  are the reference pressure and pressure, respectively;  $R$  and  $C_p$  are the gas constants and heat capacity of dry air, respectively; and  $r_v$  is the water vapour mixing ratio, with higher  $\theta_v$  indicating greater buoyancy. There is a pre-existing horizontal buoyancy gradient due to the mountains, with higher buoyancy over the mountainous regions and lower buoyancy on either side because the mountains act as an elevated heat source. This gradient is enhanced during the day (Figure 6i–j) by irrigation because the low-level areas have increased evaporative cooling, which more than offsets the buoyancy increase due to higher concentrations of water vapour. Air parcels adjacent to the mountain, particularly on the northern slopes, are more buoyant relative to their surroundings in the irrigation cases than in the control cases, increasing the probability of convection. The enhanced buoyancy gradient leads to enhanced upslope flow on both the northern and southern flanks of the plateau in the afternoon (Figure 6f), enhancing rainfall on the top of the plateau and reducing it to the south (Figure 6b).

The anomalous buoyancy gradient in the irrigation simulations reverses sign at night (Figure 6k–l), so that



the upslope buoyancy gradient is weaker at night in the irrigated simulations than in control, especially on the southern flank of the plateau. Early in the night the rainfall anomaly is predominantly over the flanks of the plateau (Figure 6c), and it propagates north and south over the irrigated plains throughout the night and into the morning (Figure 6d).

### 3.2.2 | Changes in mountain-valley flows

In the previous section we have shown that increases in rainfall on the Meghalaya plateau are preceded by

strengthened upslope flow tied to diurnally varying buoyancy gradients. We now investigate the general relationship between rainfall and upslope flow throughout the Gangetic Plain region. First we define the upslope flow parameter  $\eta$ :

$$\eta = \mathbf{u} \cdot \nabla h,$$

where  $\mathbf{u}$  is the horizontal wind vector and  $h$  is the surface elevation. Larger positive (negative) values of  $\eta$  indicate flow that is more upslope (downslope). We binned  $\eta$  by elevation from 0 to 4,000 m, with 50 m bin spacing, and by time of day, and averaged the binned  $\eta$  over 80–92°E, 22–29°E. The diurnal cycle of  $\eta$  by elevation is shown in

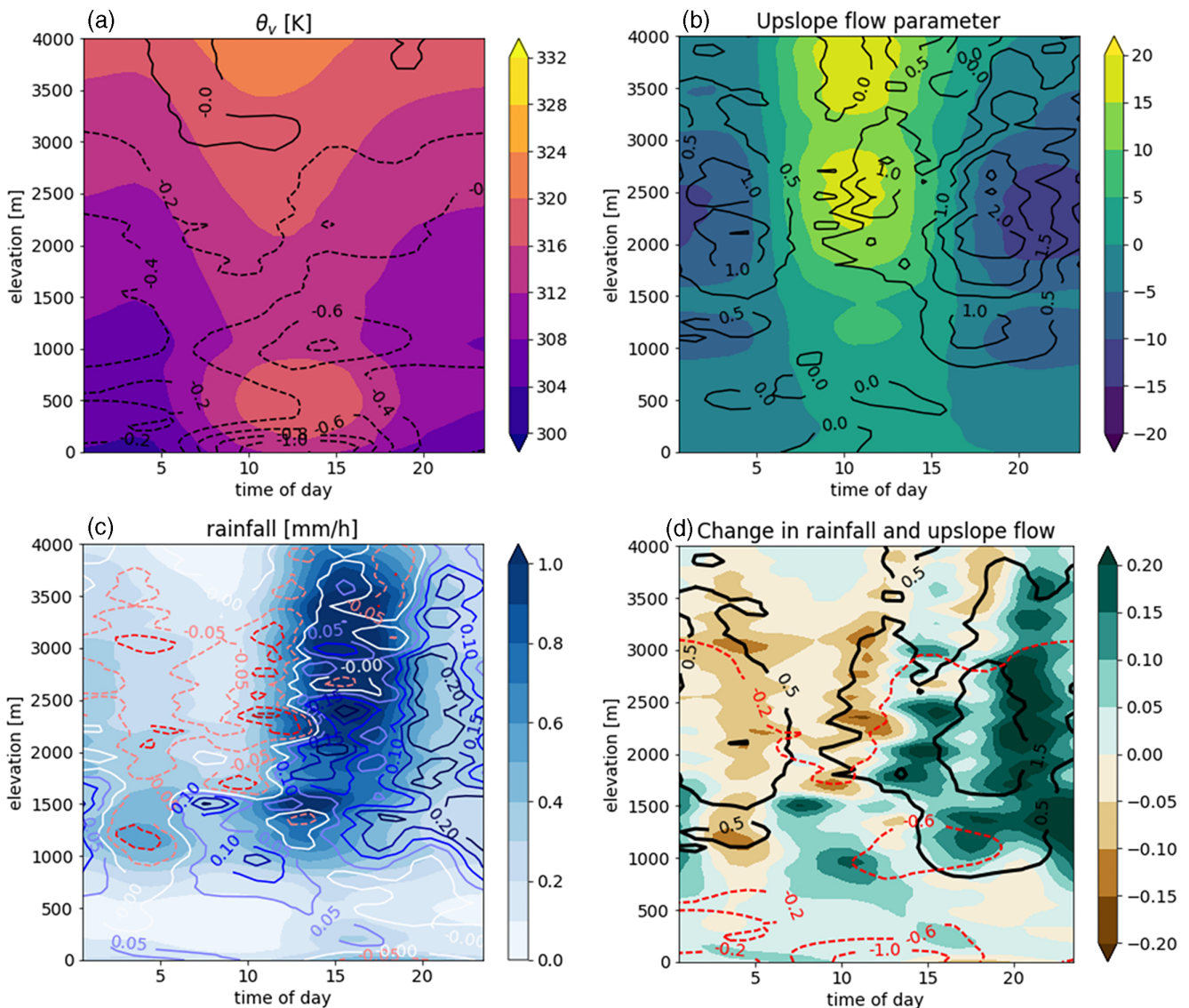


**FIGURE 7** (a) Virtual potential temperature  $\theta_v$ , (b) the upslope flow parameter  $\eta$ , and (c) rainfall, binned by time of day and elevation, across the Gangetic Plain region. In (a–c), shading shows the mean from the short control simulations while contours show the difference between irrigation and control. (d) shows these differences in rainfall (shading), upslope flow (solid contours) and  $\theta_v$  (dashed contours) [Colour figure can be viewed at [wileyonlinelibrary.com](http://wileyonlinelibrary.com)]

Figure 7 along with the rainfall and 2 m  $\theta_v$  which have been similarly binned and averaged.

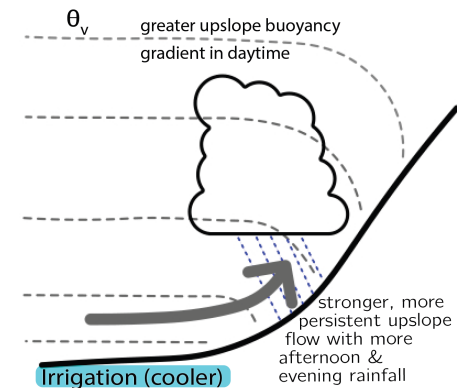
Figure 7a shows that what was seen in Figure 6 for the Meghalaya region is generally true. There is a pre-existing upslope buoyancy gradient in the control simulations which is strongest during the day. In the irrigation experiments, this gradient is enhanced during the day and slightly weakened in the early morning. Similarly, there is a peak in upslope flow (Figure 7b) during the day with downslope flow at night in the control runs. In the irrigation runs, the upslope flow change is positive on average at all times of day, so upslope flow is stronger during the day and downslope flow is weaker at night, and there is a delay in the timing of both the peak in the upslope flow and the transition from upslope to downslope flow.

There is a strong afternoon/evening peak in rainfall on elevations above about 1,000 m, with a secondary peak in the early mornings (Figure 7c). In the irrigation simulations, rainfall is suppressed in the early to mid morning and enhanced in the afternoon into early night, amplifying the diurnal cycle and delaying the peak in rainfall as with upslope flow. When the irrigation-minus-control values of all three fields are combined (Figure 7d), we see that the daytime increase in upslope flow coincides with the late morning timing of the strongest increase in the upslope buoyancy gradient, and that the enhancement of orographic afternoon rainfall occurs two to three hours later. The greatest orographic rainfall increase occurs later in the evening, coinciding with the delayed shift from upslope to downslope flow and weakening of the downslope flow; this likely increases convergence on the mountain slopes. There is some suggestion that the night-time rainfall increase on the mountains propagates down into the lowlands in the early morning and plays a role in the morning rainfall increase that occurs in the 'adjacent' region in Figure 5b.

#### 4 | SUMMARY AND CONCLUSION

We examine the effect of realistic irrigation in the Ganges basin on pre-monsoon rainfall in convection-permitting simulations. While there are many modelling studies of the effect of irrigation on the Indian monsoon, these usually use GCMs, which are known to poorly represent the response of convection to surface forcing (Taylor *et al.*, 2013; Birch *et al.*, 2015). By simulating the effect of irrigation on the pre-monsoon, during synoptically quiet periods, we isolate the effect of irrigation on local convection and mesoscale circulations, rather than on the effect of irrigation on the continental-scale monsoon circulation. By using convection-permitting simulations, we avoid the

#### (a) Afternoon and evening



#### (b) Night and early morning

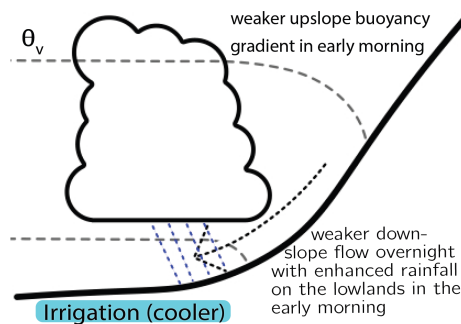


**FIGURE 8** A schematic illustration of the main ways that irrigation affects pre-monsoon rainfall in convection-permitting simulations, with enhanced buoyancy-driven upslope flow in the daytime and increased rainfall on the mountain slopes, and reduced downslope flow at night and morning, with more rainfall on the lowlands [Colour figure can be viewed at [wileyonlinelibrary.com](http://wileyonlinelibrary.com)]

errors in land-atmosphere coupling found by Taylor *et al.* (2013).

The overall effect of irrigation is to increase pre-monsoon rainfall, though this effect has considerable spatial variability. Rainfall enhancement is particularly limited by mean state humidity: much of India in the pre-monsoon is simply too dry for the moisture and circulation perturbations associated with irrigation to produce rainfall in our simulations.

The greatest absolute effect of irrigation on pre-monsoon rainfall occurs through orographic precipitation mechanisms, summarised in Figure 8. Mountains subject to strong daytime solar radiation, as in pre-monsoon India, are characterised by upslope buoyancy gradients in the day as the peaks warm faster than the valleys. This buoyancy gradient drives upslope flow with convection on the mountains during the day, and a reverse downslope flow at night. Irrigation cools the near-surface in low-lying areas, enhancing the buoyancy gradient between irrigated regions and nearby mountains.

The enhanced buoyancy gradient strengthens daytime upslope flow and delays the timing of peak upslope winds, enhancing evening rainfall on the mountains. Downslope flow overnight is also weakened.

The increase in rainfall on the irrigated regions near the mountains is most pronounced overnight and in the early morning. Irrigated regions far from orography mostly do not see an increase in rainfall, because even on the irrigated areas the rainfall increase occurs not through the local effects of moistening the column, but through the enhanced propagation of orographic rainfall downslope in the mornings. This is demonstrated by the early morning maximum of the rainfall change on the lowlands as well as the fact that increases in rainfall in lowlands occur almost exclusively in the vicinity of mountains.

The effect of irrigation on the monsoon circulation appears to be similar to those of previous studies which used coarse-scale models with cumulus convection parametrized (Saeed *et al.*, 2009; Puma and Cook, 2010; Cook *et al.*, 2014; Chou *et al.*, 2018), in the sense that the monsoon trough is weaker in the irrigation experiments for both the short and long simulations. GCM studies have attributed this weaker circulation to the continental-scale cooling caused by irrigation. However, in contrast to previous studies, in our simulations there is still an overall increase in rainfall, albeit with important spatial variability as we have described. This apparent discrepancy could be because the rainfall response to irrigation is incorrect in previous studies due to parametrized convection, which may respond incorrectly to the surface soil moisture change. However, we suspect that there is a different explanation, because previous work has shown that, in the absence of strong synoptic forcing, parametrized convective rainfall tends to increase, rather than decrease, over wetter soils (Taylor *et al.*, 2013). The fact that studies using global or regional models with parametrized convection have decreased rainfall under irrigation suggests that in those studies the rainfall change is a consequence of two competing processes: the weakening circulation (which would decrease rainfall) and the local convective response to enhanced soil moisture (which would increase rainfall under parametrized convection, possibly incorrectly), with the former dominating and leading to an overall rainfall reduction. Another possibility is that the results of Taylor *et al.* (2013) are specific to the MetUM, which they also used, although they used an earlier version of the regional model, and similar results were also seen in Hohenegger *et al.* (2009).

It is therefore likely that the overall difference between our results and those of previous studies – that is, why we see an overall increase in rainfall where previous studies see an overall decrease – is due to the season rather than convective parametrization. Based

on our and others' results cited above, we hypothesize the following. Irrigation enhances pre-monsoon rainfall, which is driven primarily by local convection and mesoscale circulations, while it reduces monsoon rainfall by weakening the large-scale circulation and delaying monsoon onset. This is consistent with the observational findings of Niyogi *et al.* (2010) and is plausibly consistent with the GCM findings of Chou *et al.* (2018), who saw a rainfall increase in some parts of South Asia in May due to irrigation despite an overall decrease in summer monsoon rainfall. Our hypothesis would be best explored with an ensemble of longer-running convection-permitting experiments which covered at least one full monsoon season and had realistic irrigation, as was used in our short experiments. The time evolution of our long experiment (Figure 3) plausibly suggests that longer-running versions of those short experiments would show a larger-magnitude response than we found in the three-day integrations.

Furthermore, previous studies did not discuss the effect of irrigation on orographic precipitation. Here it is likely that mountain-valley flows and the convective response to irrigation-induced changes in such flows must be resolved by the model, and it is known that parametrized convection does not represent such responses correctly (Birch *et al.*, 2015). Chou *et al.* (2018) did find (but did not discuss) a rainfall increase over some mountainous areas, but these appear more to be an orographic enhancement of a general east–west tripole pattern in the rainfall response to irrigation (their Figure 3).

If irrigation increases pre-monsoon orographic precipitation, it likely increases the chance of extreme rainfall leading to flash floods and landslides. This physical mechanism need not be limited to India and could in fact operate in many locations where irrigation occurs near mountain ranges. Irrigation has the potential to alter the local-, regional-, and continental-scale climate in a variety of ways; to our knowledge its effect on orographic precipitation has not previously been evaluated.

## AUTHOR CONTRIBUTIONS

**J. K. Fletcher:** conceptualization; formal analysis; funding acquisition; investigation; methodology; project administration; validation; visualization. **C. E. Birch:** conceptualization; data curation; funding acquisition; methodology; resources. **R. J. Keane:** data curation; methodology; project administration; resources. **C. M. Taylor:** conceptualization; formal analysis; funding acquisition; methodology; resources. **S. S. Folwell:** data curation; formal analysis; methodology; validation; visualization.

## ACKNOWLEDGEMENTS

We acknowledge funding from the Newton Fund, WCSSP India WP2 Lots 3 and 4, and UK Natural Environment Research Council NE/L013843/1 (University of Leeds) and NE/L013819/1 (UK Centre for Ecology and Hydrology).

## ORCID

J. K. Fletcher  <https://orcid.org/0000-0002-4892-3344>  
 C. E. Birch  <https://orcid.org/0000-0001-9384-2810>  
 R. J. Keane  <https://orcid.org/0000-0002-7506-7352>  
 C. M. Taylor  <https://orcid.org/0000-0002-0120-3198>  
 S. S. Folwell  <https://orcid.org/0000-0001-5745-4116>

## REFERENCES

- Barton, E.J., Taylor, C.M., Parker, D.J., Turner, A.G., Belušić, D., Böing, S.J., Brooke, J.K., Chawn Harlow, R., Harris, P.P., Hunt, K., Jayakumar, A. and Mitra, A.K. (2020) A case-study of land–atmosphere coupling during monsoon onset in northern India. *Quarterly Journal of the Royal Meteorological Society*, 146, 2891–2905.
- Best, M.J., Pryor, M., Clark, D.B., Rooney, G.G., Essery, R., Ménard, C.B., Edwards, J.M., Hendry, M.A., Porson, A., Gedney, N., Mercado, L.M., Sitch, S., Blyth, E., Boucher, O., Cox, P.M., Grimmond, C.S.B. and Harding, R.J. (2011) The joint UK land environment simulator (JULES), model description-Part 1: energy and water fluxes. *Geoscientific Model Development*, 4(3), 677–699.
- Bhat, G.S., Morrison, R., Taylor, C.M., Bhattacharya, B.K., Paleri, S., Desai, D., Evans, J.G., Pattnaik, S., Sekhar, M., Nigam, R., Sattar, A., Angadi, S.S., Kacha, D., Patidar, A., Tripathi, S.N., Krishnan, K.V.M. and Sisodiya, A. (2020) Spatial and temporal variability in energy and water vapour fluxes observed at seven sites on the Indian subcontinent during 2017. *Quarterly Journal of the Royal Meteorological Society*, 146, 2853–2866.
- Birch, C.E., Roberts, M.J., Garcia-Carreras, L., Ackerley, D., Reeder, M.J., Lock, A.P. and Schiemann, R. (2015) Sea-breeze dynamics and convection initiation: the influence of convective parameterization in weather and climate model biases. *Journal of Climate*, 28(20), 8093–8108. <https://doi.org/10.1175/jcli-d-14-00850.1>.
- Bush, M., Allen, T., Bain, C., Boutle, I., Edwards, J., Finnenkoetter, A., Franklin, C., Hanley, K., Lean, H.W., Lock, A.P., Manners, J., Mittermaier, M., Morcrette, C.J., North, R., Petch, J., Short, C., Vosper, S., Walters, D., Webster, S., Weeks, M., Wilkinson, J., Wood, N. and Zerroukat, M. (2020) The first Met Office Unified Model–JULES regional atmosphere and land configuration, RAL1. *Geoscientific Model Development*, 13(4), 1999–2029.
- Chou, C., Ryu, D., Lo, M.H., Wey, H.W. and Malano, H.M. (2018) Irrigation-induced land–atmosphere feedbacks and their impacts on Indian summer monsoon. *Journal of Climate*, 31(21), 8785–8801. <https://doi.org/10.1175/jcli-d-17-0762.1>.
- Cook, B.I., Shukla, S.P., Puma, M.J. and Nazarenko, L.S. (2014) Irrigation as an historical climate forcing. *Climate Dynamics*, 44(5–6), 1715–1730. <https://doi.org/10.1007/s00382-014-2204-7>.
- Douglas, E.M., Niyogi, D., Frolking, S., Yeluripati, J.B., Pielke, R.A.Sr., Niyogi, N., Vörösmarty, C.J. and Mohanty, U.C. (2006) Changes in moisture and energy fluxes due to agricultural land use and irrigation in the Indian monsoon belt. *Geophysical Research Letters*, 33(14). <https://doi.org/10.1029/2006GL026550>.
- Douglas, E.M., Beltrán-Przekurat, A., Niyogi, D., Pielke, R.A. and Vörösmarty, C.J. (2009) The impact of agricultural intensification and irrigation on land–atmosphere interactions and Indian monsoon precipitation – a mesoscale modeling perspective. *Global and Planetary Change*, 67(1–2), 117–128. <https://doi.org/10.1016/j.gloplacha.2008.12.007>.
- Guimberteau, M., Laval, K., Perrier, A. and Polcher, J. (2011) Global effect of irrigation and its impact on the onset of the Indian summer monsoon. *Climate Dynamics*, 39(6), 1329–1348. <https://doi.org/10.1007/s00382-011-1252-5>.
- Hersbach, H., Bell, B., Berrisford, P., Hirahara, S., Horányi, A., Muñoz-Sabater, J., Nicolas, J., Peubey, C., Radu, R., Schepers, D., Simmons, A., Soci, C., Abdalla, S., Abellan, X., Balsamo, G., Bechtold, P., Biavati, G., Bidlot, J., Bonavita, M., De Chiara, G., Dahlgren, P., Dee, D.P., Diamantakis, M., Dragani, R., Flemming, J., Forbes, R., Fuentes, M., Geer, A.J., Haimberger, L., Healy, S.B., Hogan, R.J., Hólm, E.V., Janisková, M., Keeley, S., Laloyaux, P., Lopez, P., Lupu, C., Radnoti, G., de Rosnay, P., Rozum, I., Vamborg, F., Villaume, S. and Thépaut, J.-N. (2020) The ERA5 global reanalysis. *Quarterly Journal of the Royal Meteorological Society*, 146, 1999–2049.
- Hohenegger, C., Brockhaus, P., Bretherton, C.S. and Schär, C. (2009) The soil moisture–precipitation feedback in simulations with explicit and parameterized convection. *Journal of Climate*, 22(19), 5003–5020.
- Huffman, G.J., Bolvin, D.T., Braithwaite, D., Hsu, K., Joyce, R., Xie, P. and Yoo, S.-H. (2015) NASA global precipitation measurement (GPM) integrated multi-satellite retrievals for GPM (IMERG); Algorithm Theoretical Basis Document (ATBD) version 4.5, Greenbelt, MD.
- Hunt, K.M.R. and Fletcher, J.K. (2019) The relationship between Indian monsoon rainfall and low-pressure systems. *Climate Dynamics*, 53(3–4), 1859–1871.
- Islam, M.N. (2007) *Review of International Watercourses Law for the 21st Century: the Case of the River Ganges Basin*. Subedi, S.P. (ed.) *Journal of Environmental Law*, 19(1), 143–145. <https://doi.org/10.1093/jel/eqj027>.
- Koster, R.D., Dirmeyer, P.A., Guo, Z., Bonan, G., Chan, E., Cox, P., Gordon, C.T., Kanae, S., Kowalczyk, E., Lawrence, D., Liu, P., Lu, C.H., Malyshev, McAvaney, B., Mitchell, K., Mocko, D., Oki, T., Oleson, K., Pitman, A., Sud, Y.C., Taylor, C.M., Verseghy, D., Vasic, R., Xue, Y. and Yamada, T. (2004) Regions of strong coupling between soil moisture and precipitation. *Science*, 305, 1138–1140. <https://doi.org/10.1126/science.1100217>.
- Lee, E., Chase, T.N., Rajagopalan, B., Barry, R.G., Biggs, T.W. and Lawrence, P.J. (2009) Effects of irrigation and vegetation activity on early Indian summer monsoon variability. *International Journal of Climatology*, 29(4), 573–581. <https://doi.org/10.1002/joc.1721>.
- Mann, H.B. and Whitney, D.R. (1947) On a test of whether one of two random variables is stochastically larger than the other. *Annals of Mathematical Statistics*, 18, 50–60. <https://doi.org/10.1214/aoms/1177730491>.
- Martin, G.M., Brooks, M.E., Johnson, B., Milton, S.F., Webster, S., Jayakumar, A., Mitra, A.K., Rajan, D. and Hunt, K.M.R. (2020) Forecasting the monsoon on daily to seasonal time-scales in support of a field campaign. *Quarterly Journal of the Royal*

- Meteorological Society*, 146, 2906–2927. <https://doi.org/10.1002/qj.3620>.
- Mitra, A.K., Bohra, A.K., Rajeevan, M.N. and Krishnamurti, T.N. (2009) Daily Indian precipitation analysis formed from a merge of rain-gauge data with the TRMM TMPA satellite-derived rainfall estimates. *Journal of the Meteorological Society of Japan. Series II*, 87A, 265–279. <https://doi.org/10.2151/jmsj.87A.265>.
- Niyogi, D., Kishtawal, C., Tripathi, S. and Govindaraju, R.S. (2010) Observational evidence that agricultural intensification and land use change may be reducing the Indian summer monsoon rainfall. *Water Resources Research*, 46(3). <https://doi.org/10.1029/2008WR007082>.
- Puma, M.J. and Cook, B.I. (2010) Effects of irrigation on global climate during the 20th century. *Journal of Geophysical Research*, 115(D16). <https://doi.org/10.1029/2010jd014122>.
- Rajeevan, M., Gadgil, S. and Bhate, J. (2010) Active and break spells of the Indian summer monsoon. *Journal of Earth System Science*, 119(3), 229–247.
- Rodell, M., Houser, P.R., Jambor, U.E.A., Gottschalck, J., Mitchell, K., Meng, C.-J., Arsenault, K., Cosgrove, B., Radakovich, J., Bosilovich, M., Entin, J.K., Walker, J.P., Lohmann, D. and Toll, D. (2004) The global land data assimilation system. *Bulletin of the American Meteorological Society*, 85(3), 381–394.
- Sacks, W.J., Cook, B.I., Buening, N., Levis, S. and Helkowski, J.H. (2008) Effects of global irrigation on the near-surface climate. *Climate Dynamics*, 33(2–3), 159–175. <https://doi.org/10.1007/s00382-008-0445-z>.
- Saeed, F., Hagemann, S. and Jacob, D. (2009) Impact of irrigation on the South Asian summer monsoon. *Geophysical Research Letters*, 36(20). <https://doi.org/10.1029/2009gl040625>.
- Shukla, S.P., Puma, M.J. and Cook, B.I. (2013) The response of the South Asian Summer Monsoon circulation to intensified irrigation in global climate model simulations. *Climate Dynamics*, 42(1–2), 21–36. <https://doi.org/10.1007/s00382-013-1786-9>.
- Siebert, S., Kummu, M., Porkka, M., Döll, P., Ramankutty, N. and Scanlon, B.R. (2015) A global data set of the extent of irrigated land from 1900 to 2005. *Hydrology and Earth System Sciences*, 19, 1521–1545. <https://doi.org/10.5194/hess-19-1521-2015>.
- Taylor, C.M., de Jeu, R.A.M., Guichard, F., Harris, P.P. and Dorigo, W.A. (2012) Afternoon rain more likely over drier soils. *Nature*, 489(7416), 423–426. <https://doi.org/10.1038/nature11377>.
- Taylor, C.M., Birch, C.E., Parker, D.J., Dixon, N., Guichard, F., Nikulin, G. and Lister, G.M.S. (2013) Modeling soil moisture–precipitation feedback in the Sahel: importance of spatial scale versus convective parameterization. *Geophysical Research Letters*, 40(23), 6213–6218. <https://doi.org/10.1002/2013gl058511>.
- Tuinenburg, O.A., Hutjes, R.W.A., Stacke, T., Wiltshire, A. and Lucas-Picher, P. (2014) Effects of irrigation in India on the atmospheric water budget. *Journal of Hydrometeorology*, 15(3), 1028–1050.
- Turner, A.G., Bhat, G.S., Martin, G.M., Parker, D.J., Taylor, C.M., Mitra, A.K., Tripathi, S.N., Milton, S.F., Rajagopal, E.N., Evans, J.G., Morrison, R., Pattnaik, S., Sekhar, M., Bhattacharya, B.K., Madan, R., Govindankutty, M., Fletcher, J.K., Willetts, P.D., Menon, A. and Marsham, J.H. (2020) Interaction of convective organization with monsoon precipitation, atmosphere, surface and sea: the 2016 INCOMPASS field campaign in India. *Quarterly Journal of the Royal Meteorological Society*, 146, 2828–2852. <https://doi.org/10.1002/qj.3633>.
- Weedon, G.P., Gomes, S., Viterbo, P., Shuttleworth, W.J., Blyth, E., Österle, H., Adam, J.C., Bellouin, N., Boucher, O. and Best, M. (2011) Creation of the WATCH forcing data and its use to assess global and regional reference crop evaporation over land during the twentieth century. *Journal of Hydrometeorology*, 12(5), 823–848.

**How to cite this article:** Fletcher, J.K., Birch, C.E., Keane, R.J., Taylor, C.M. & Folwell, S.S. (2021) The effect of Ganges river basin irrigation on pre-monsoon rainfall. *Quarterly Journal of the Royal Meteorological Society*, 1–15. Available from: <https://doi.org/10.1002/qj.4218>

## APPENDIX A. CREATING SOIL MOISTURE DATASETS

Determining the impact of irrigation on atmospheric circulations and rainfall across Northern India is the aim of our study. However our land surface model does not explicitly represent irrigation, so we mimic the effect of irrigation patterns by adjusting the soil moisture. This Appendix describes how we created the maps of soil moisture that provide the lower boundary conditions for the atmospheric model.

Analysis of MODIS Terra land surface temperatures (LST) sampled at approximately 1030 LT provide a reliable indication of where increased soil moisture maintains evapotranspiration and cools the surface. The May climatology (Figure A1) identifies strong spatial contrasts of up to 10 K in pre-monsoon LST associated with flood irrigation. The climatological LST pattern for June is similar, though the advance of monsoon rains from the south-east introduces an additional source of soil moisture not directly related to irrigation. Maps of areas equipped for irrigation (Siebert *et al.*, 2015) are quite consistent with the structures picked out in the LST climatology. This justifies our approach and, importantly, demonstrates the ready availability of water for evapotranspiration during our period of interest.

To assess the atmospheric impact of this complex irrigation pattern, we superimposed a pattern of additional soil moisture (based on the LST climatology) onto a realistic soil moisture field. The latter “control” soil moisture map was generated by running an offline version of the Joint UK Land Environment Simulator (JULES; Best *et al.*, 2011) with observationally based atmospheric forcing and the prescribed uniform sandy soil properties. In

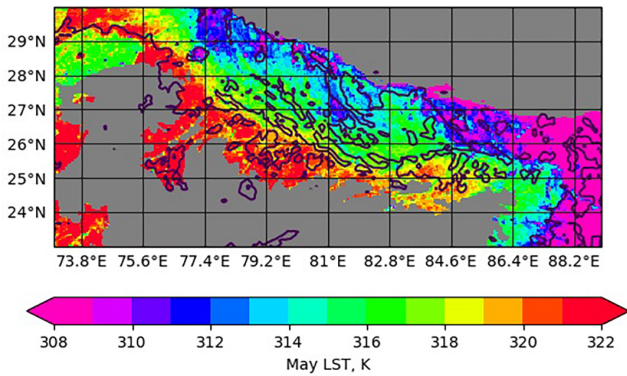


**FIGURE A1** The MODIS Terra LST May climatology (shading) with contours showing areas at least 50% equipped for irrigation. Grey shading is applied to pixels above 300 m above mean sea level. [Colour figure can be viewed at [wileyonlinelibrary.com](http://wileyonlinelibrary.com)]

the “irrigated” soil moisture fields, we increase soil moisture in pixels where the May LST value falls below a certain threshold (details below). We exclude pixels above 300 m altitude to minimise the impact of reduced LST with topographic height.

### A.1 Control soil moisture

To create the control soil moisture for the month-long atmospheric simulation, we use JULES and the same land configuration as in the atmospheric model but forced with Watch Forcing Data Era Interim (Weedon *et al.*, 2011). This is a global dataset with bias correction of monthly rainfall, rain days and temperature. The offline model was run for several annual cycles until soil moisture was spun up, that is, the soil moisture in each grid box is within 1% of the previous initial cycle value. The monthly mean soil moisture from the most recent five years (2009 to 2014) of the run was taken, providing climatological values. Finally, the soil moisture dataset is regridded using bilinear interpolation to the atmospheric model resolution (4.4 km). The bilinear interpolation also reduces the impact of the coarse grid box boundaries appearing in the soil moisture and surface fluxes in the higher-resolution atmospheric model. In the long runs, soil moisture in the atmospheric model is updated every midnight, linearly interpolating from the monthly values. For the short runs, the soil moisture in the control dataset more accurately represent the evolving conditions in a specific year (2016). This was achieved by driving the offline model with a 0.25° daily merged satellite and gauged rainfall product (Mitra *et al.*, 2009) from 1 October 2015. Additional forcing variables were taken from the Global Land Data Assimilation System (GLDAS2.1; Rodell *et al.*, 2004) reanalysis product to create the 3-hourly data for JULES. With greater confidence in the day-to-day soil moisture patterns being produced

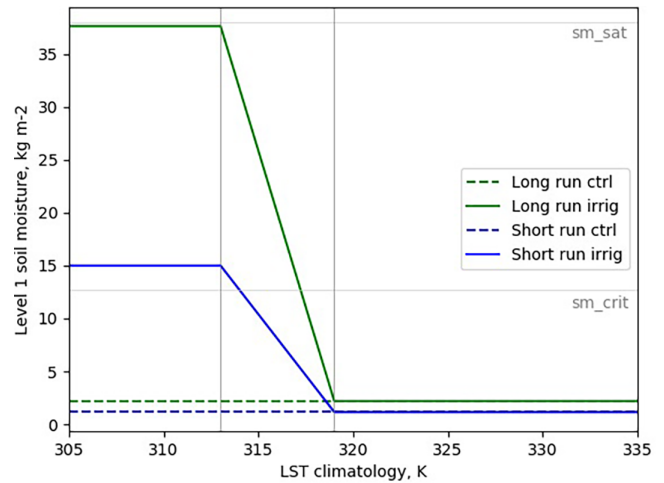


**FIGURE A2** Functional relationships for soil moisture and LST climatology used in the control and perturbed runs, illustrated here for level 1 soil moisture. The horizontal lines (grey) indicate the soil water saturation and critical points for sand [Colour figure can be viewed at [wileyonlinelibrary.com](http://wileyonlinelibrary.com)]

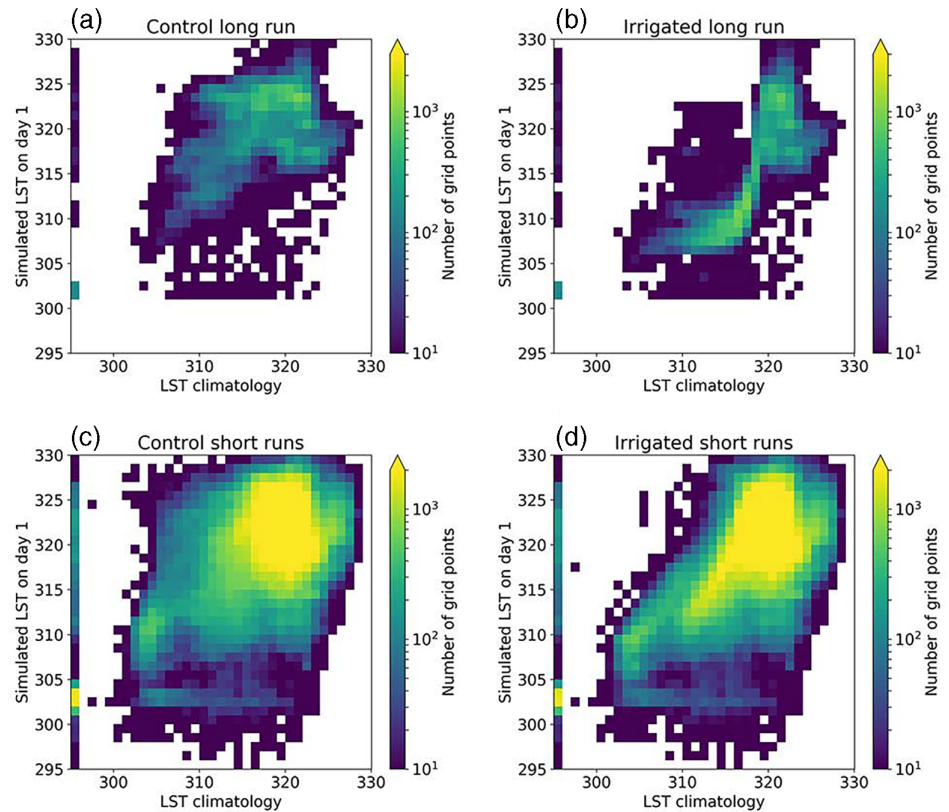
offline (outside the irrigated areas) we took those daily values to initialise the atmospheric model. Unlike in the month-long irrigated simulation, once initialised the soil moisture evolved freely in response to model physics in the 3-day simulations.

### A.2 Irrigation soil moisture

We created soil moisture fields for the irrigation runs using simple piece-wise linear relationships between the climatological LST and soil moisture (Figure A2). Here, the unperturbed (or control) soil moisture is the mean soil moisture across all pixels where LST<sub>MAY</sub>, the climatological May LST, is below 319 K. In the long run, the soil moisture in all soil levels was increased to just below the soil saturation point wherever LST<sub>MAY</sub> is below 313 K, and decreasing adjustments with LST in the range 313 to 319 K (Figure A2). These thresholds were chosen based on visual comparison between the area equipped for irrigation and climatological LST in Figure A1.

Having run the atmospheric model with both the control and irrigation soil moisture initialisations, we compared simulated and observed LSTs across the domain. The modelled LSTs were sampled at 1030 LT under approximately clear-sky conditions (downward short-wave radiation at the surface is greater than 90% of downward clear-sky short-wave radiation). Density plots of modelled and observed LST (Figure A3a, b) show the extent to which we have cooled the surface through adding water to the soil stores. There is almost no relationship between modelled and observed LST in the control run. This indicates that the combination of atmospheric forcing and vegetation and

**FIGURE A3** Density plots showing the LST climatology versus modelled LST from day 1 of (a, b) the long runs and (c, d) short runs showing (a, c) the control run and (b, d) perturbed soil moisture [Colour figure can be viewed at [wileyonlinelibrary.com](http://wileyonlinelibrary.com)]



soil properties cannot produce the strong LST contrasts we observe in Figure A1. By design, a much stronger positive relationship emerges in the irrigation run. There is a clear impact on surface temperatures, where we have suppressed model temperatures by up to 15 K in the observed climatology range 319 to 313 K. The rather sharp threshold in Figure A3b for observed LSTs above 319 K implies that the irrigation increment applied was excessive for climatological LSTs between 313 and 319 K. The implication of that for the month-long atmospheric simulation is that the surface flux perturbations are also unrealistically excessive in the irrigation scenario.

The short simulations provided an opportunity to refine the soil moisture constraint for the irrigation case. Accordingly we applied a more subtle irrigation increment (Figure A2). Rather than setting the coolest pixels close to

saturation, we reduced the soil moisture to 0.15 mm water per mm soil, just above the critical point of 0.127 mm water per mm soil, applying this change to the top three soil levels (1 m). This means there is sufficient water to maintain evapotranspiration over the three days of simulation for the coolest pixels, as the critical point marks the onset of vegetation water stress. However, relative to the long irrigated simulation, it reduces the contribution of bare soil evaporation, which in JULES continues for soil moisture above the critical point. The density plots of modelled land surface temperature show a much improved distribution of modelled LST in the irrigated simulation (Figure A3), with cooling of the warmer pixels of only up to 10 K. This implies that the surface flux forcing in the irrigated short runs is of a realistic magnitude.